RAMReS Sciences des Structures et de la Matière Vol. 6, N°1 (2022) 15 - 29
http://publication.lecames.org/index.php/mat ISSN: 2630-1180

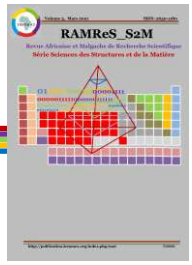

Spectroscopic characterizations and sum-frequency generation of chiral binaphthol derivatives

Kossivi Bienvenu Rodrigue Afoudji[1], Julien Egly[2], Milohum Mikesokpo Dzagli[1,*], Stéphane Bellemin-Laponnaz[2], Kokou Dodzi Dorkenoo[2]

[1]*Laboratoire de Physique des Matériaux et des Composants à Semi-conducteurs (LPMCS), Département de Physique, Université de Lomé, Lomé, Togo*
[2]*Université de Strasbourg, CNRS, Institut de Physique et Chimie des Matériaux de Strasbourg, UMR 7504, Strasbourg 67000, France*

Received: 17 February 2022 / Received in revised form: 4 April 2022 / Accepted: 27 April 2022

***Abstract*:**

Research concerning the enantiomers of chiral active compounds and especially their separations constituted a major challenge for drugs design. It is crucial to study the chirality of molecules for their applications. This study aims to investigate chirality in liquid media containing enantiopure chiral molecules from derivatives of binaphthol through sum-frequency generation microscopy and spectroscopic techniques. Derivatives of binaphthol, obtained by substituting the hydrogen atoms of hydroxyl group (-OH) with alkyl groups: (-CH_3) and (-$C_{22}H_{45}$), were studied using UV visible spectroscopy, NMR, IR transmission, Raman and sum-frequency generation microscopy (SFG). Modifications of chemical bonds which took place on the molecule of binaphthol were performed and highlighted by IR and Raman measurements. On IR and Raman spectra, bands related to (-OH) group vibrations (1382 cm^{-1}, 3429 cm^{-1} and 3507 cm^{-1}) disappeared while bands corresponding to alkyl chains vibration modes appeared (708 cm^{-1}, 2848 cm^{-1} and 2915 cm^{-1}). Chiral SFG spectra and images were then performed on the functionalized R Binol-C_{22} sample. Good contrasts were obtained in appropriate configurations of the sum-frequency generator device. Chiral compounds R Binol-C_{22} were detected using Sum-frequency generation imaging and spectroscopy. The information obtained by sum-frequency generation is of great importance to the community.

***Keywords*:** Binol; Chirality; Sum-frequency generation.

*Corresponding author:
Email address: mdzagli@gmail.com *(M.M. Dzagli)*

1. Introduction

Chirality is of paramount importance for chemists and biologists and in pharmacology. The chirality of reactants influences asymmetric synthetic chemical and enzymatic reactions. The stereochemical nature of a molecule determines its chemical, biochemical, pharmacological and pharmacokinetic properties and its toxicity. Nowadays, several active therapeutic compounds present chirality and are found in a racemic mixture in drugs [1, 2]. Thus, the search on chiral separation of racemic mixtures of pharmaceuticals are becoming a real challenge in the design of drugs. There is considerable demand for separation techniques appropriate of chiral molecules [3]. The chirality of molecules is determined by the measurement of circular dichroism which is also limited, because the quantities measured are linked to the electric quadrupole and are generally low. An efficient chiral separation method of pharmaceuticals would be useful for commercial systems in the future. The understanding of certain nonlinear optical properties has made it possible to develop techniques for characterizing matter [4, 5]. Thus, it has been shown that it is possible to generate sum-frequency signals in chiral isotropic media [6, 7] and this has fostered a new technique for studies of chiral molecules. This sum-frequency generation (SFG) technique in chiral liquids is interesting, because the signal obtained is only related to chirality, given that isotropic media like all centrosymmetric media have zero quadratic susceptibility [8, 9]. The calculation of the chiral quadratic susceptibility also shows that this susceptibility cannot generate all quadratic phenomena. The expression of the quadratic chiral susceptibility is given by Eq. (1) [10]. The second harmonic generation is prohibited because of the factor (ω_2-ω_1) which cancels the susceptibility when the frequencies of the two waves are equal. 2,2-dihydroxy-1,1-binaphthyl (Binol) is the first chiral molecule on which electron resonance SFG was first performed [11]. Binol is an archetypal chiral molecule with an unsymmetrical chromophore composed of two aromatic rings. Chirality study models developed with circular dichroism on molecules with similar structures have contributed to the determination of the absolute configurations and conformations of several organic compounds in solution [12]. The general objective of the present study is to evaluate the conservation of the chirality of the molecules derived from Binol by sum-frequency generation and spectroscopic techniques.

To do this, the derivatives of the R enantiomer of Binol, were obtained by substituting the hydrogen atoms of (-OH) groups by the methyl group (-CH_3) and the Docosyl group (-$C_{22}H_{45}$).

$$\chi^{(2)}_{chiral}(\omega_1+\omega_2,\omega_2,\omega_1)=\frac{N}{12\hbar^2\varepsilon_0}\sum_{mn}\left[\frac{(\omega_2-\omega_1)\left(\mu_{gn}.(\mu_{nm}\times\mu_{mg})\right)}{(\omega_1+\omega_2-\omega_{ng}+i\Gamma_{ng})(\omega_2-\omega_{mg}+i\Gamma_{mg})(\omega_1-\omega_{mg}+i\Gamma_{mg})}\right] \quad (1)$$

Characterizations were carried out by spectroscopic techniques (UV-visible, NMR, IR and Raman) and sum-frequency generation microscopy. These Binol derivatives obtained constitute intermediate reagents for the synthesis of the sulphonate derivatives of Binol and of the chiral surfactant compounds for the asymmetric reactions.

2. Materials and methods

2.1. Sum-frequency generation microscope

The sum-frequency generation was performed by superposition of two laser beams on the sample. The first beam of wavelength of 900 nm was produced by a titanium sapphire pulse laser (Tsunami, Spectra-Physics) with a duration of 80 fs at a repetition rate of 80 MHz. The second beam, 450 nm of wavelength was produced by second harmonic generation induced in barium beta borate (BBO) crystal by a part of the first beam.

A delay line was made on the 900 nm beam path to have time coincidence. The two beams were then collimated and directed towards an inverse microscope (Olympus IX71) with a spacing of 4 mm beam's width, then were focused on the sample through an immersion microscope objective (Olympus, 60x, NA 1.42). The SFG signal emitted at 300 nm was detected in transmission using a CaF_2 objective (LMU UVB 40x) with good UV transmission. A polarizer placed in front of the detectors made it possible to select the desired polarization configuration. The beam passed through a filter to cut the excitation wavelengths and the SFG signal was recorded by the detection system which was composed of a CCD camera and a photomultiplier coupled to a spectrometer. Polarizers and the delay line installed in the path of the 900 nm beam allowed different configurations for the device. It could be:

- SPP_zero, the configuration in which the output polarization is perpendicular to the input polarizations and the delay line is in the position where there is coherence between the two incident beams;
- SPP_off_zero, the configuration in which the output polarization is perpendicular to the input polarizations and the delay line is in the position where there is no coherence between the two incident beams;
- PPP_zero, the configuration in which the output polarization is parallel to the input polarizations and the delay line is in the position where there is coherence between the two incident beams;
- PPP_off_zero, the configuration in which the output polarization is parallel to the input polarizations and the delay line is in the position where there is no coherence between the two incident beams.

2.2. Spectroscopic measurements

2.2.1. Instrumentation

The UV-Visible absorption were carried out using a Cary 100 Agilent Technologies spectrophotometer with a spectral range from

190 to 900 nm. This spectrophotometer, with an accuracy of ± 2 nm, has a working range beyond 3.5 absorbance units which allowed working with more concentrated solutions. The light source was a tungsten halogen lamp. The Raman Spectrometer, model RS 201819, with a spectral range from 200 to 3700 cm^{-1} was used for Raman spectra measurements. The excitation source was a laser emitting at 785 nm with an adjustable power that can reach a maximum value of 450 mW. For IR-spectrum measurement, the Perkin Elmer Spectrum Two FT-IR-spectrometer was used. This spectrometer had an optical system with KBr windows for data collection over a spectral range of 8300 to 350 cm^{-1} with a resolution of 0.5 cm^{-1}. The MNR-spectra were carried out using Bruker Avance III HD - 500 MHz.

2.2.2. Characterization protocol

For UV visible absorbance measurements, each compound of the study was dissolved in chloroform at a concentration of 0.45 mmol/L. Liquid samples were collected in quartz cuvettes for analysis. For sum-frequency generation, R Binol-C_{22} molecules were dissolved in tetrahydrofuran at a concentration of 0.25 mol/L. The liquid solution was then deposited on a microscope slide and covered with a coverslip. The edges were sealed with a resin. The prepared sample was placed on the object stage of the microscope in such a way that the coverslip was oriented downwards. The objective for focusing the incident beams was therefore in contact with the coverslip. The samples were taken for analysis with the Raman spectrometer and were placed under the probe of the spectrometer. The probe was adjusted to the optimal position of the surface of the sample and the spectrum was collected using “Rspec” software. The IR spectra were obtained by total attenuated reflectance (ATR) technique. For NMR spectrum measurements, the molecules are dissolved in chloroform and then placed in the sample holder. Few milligrams (5 to 10 mg) of sample were dissolved in deuteured chloroform (0.6 mL). The clear solution was placed in a NMR glass tube. The tube was placed in the NMR-spectrometer then the magnetic field was adjusted to the sample (lock and shim).

Then the acquisition began and stopped after 16 scans for ^{1}H NMR or after 1024 scans for ^{13}C NMR at 298K. The acquisition signals were processed with a specific software to obtain the different spectra. The ^{1}H and ^{13}C $\{^{1}H\}$ nuclear magnetic resonance (NMR) spectra were recorded. ^{13}C assignments were confirmed when necessary using DEPT 135 experiments. ^{1}H and ^{13}C NMR-spectra were referenced using the residual solvent peak (CDCl3: δ_H = 7.26 ppm; δ_C = 77.16 ppm) at 295K.

2.3. Synthesis of Binol derivatives

The synthesis of Binol derivatives was carried out. The general equation of the reaction is given in figure 1 where RI is alkyl iodide with R corresponding to methyl group (-CH_3) or

Docosyl group (-$C_{22}H_{45}$), K_2CO_3 is potassium carbonate.

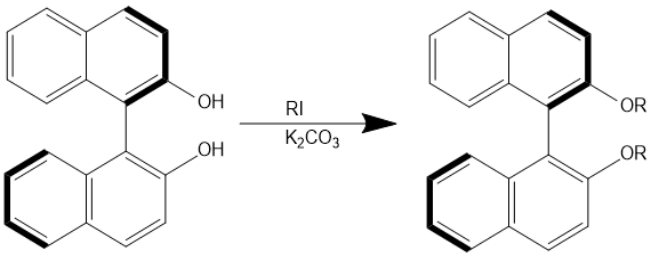

Fig. 1. Synthesis reaction scheme of derivatives of binaphthol.

2.3.1. Synthesis of R Binol-C

The synthesis of Binol derivatives was carried out as follows: a mixture of the R enantiomer of 2,2-dihydroxy-1,1-binaphthyl (Binol) (1 g; 3.5 mmol, 1 equiv), of iodomethane (1.98 g; 14 mmol, 4 equiv) and K_2CO_3 (1.93 g; 14 mmol; 4 equiv) in anhydrous acetone (30 mL) was refluxed for 18 hours. The mixture was then cooled to ambient temperature and the solvent was evaporated under vacuum. The resulting product was then taken up in 50 mL of an ethyl acetate: water (1:1) mixture. The organic phase was then washed twice with distilled water and once with brine. The organic phase was then dried over Na_2SO_4, filtered and the solvent was evaporated under vacuum. The residue was purified by column chromatography on SiO_2 using hexane/Dichloromethane v/v (2:1) to pure Dichloromethane as eluent. 639 mg of the product were obtained with a yield of 58%. This product appeared in the form of a white powder which was used for the various characterizations [13]. The peaks assigned to R Binol-C**,** are listed as follows: ^{1}H NMR (500 MHz, CDCl3, 20 °C): δ 3.77 (s, 6H), 7.11 (d, J = 8.8 Hz, 2H), 7.20-7.22 (dd, J = 6.9 Hz, 1.2 Hz, 2H), 7.31-7.32 (dd, J = 6.9 Hz, 1.3 Hz, 2H), 7.46 (d, J = 9.0 Hz, 2H), 7.87 (d, J = 9.0 Hz, 2H), 7.98 (d, J = 7.5 Hz, 2H) ppm[1]. ^{13}C NMR (125 MHz, $CDCl_3$, 20 °C): δ 56.85, 114.18, 119.53, 123.43, 125.18, 126.22, 127.85, 129.15, 129.32, 133.94, 154.90 ppm. These NMR data were similar to those of Ankireddy et al. [14].

2.3.2. Synthesis of R Binol-C_{22}

The synthesis of this Binol derivative was carried out as follows: a mixture of the R enantiomer of 2,2 dihydroxy-1,1-binaphthyl (Binol) (0.5 g; 1.75 mmol, 1 equiv), of 1-bromodocosane (1.36 g; 3.5 mmol, 2 equiv) and K_2CO_3 (1.75 g; 12.68 mmol; 7.25 equiv) was realised in anhydrous Dimethylformamide (30 mL) and was heated at 80 °C for 18 hours. The mixture was then cooled to room temperature and the solvent was evaporated under vacuum at 50 °C. The resulting product was taken up to 100 mL of an ethyl acetate: water (1:1) mixture. The organic phase was washed twice with distilled water and once with brine. The organic phase was dried over Na_2SO_4, filtered and the solvent is evaporated under vacuum. The residue was purified by column chromatography on SiO_2 using a pure hexane to hexane: ethyl acetate v/v (50:1) as eluent. 830 mg (52%) of the product were obtained. This product appeared in the form

[1] δ= chemical shifts, J= coupling constants. Abbreviations for multiplicity observed signals: s = singlet, d = doublet, t = triplet, dd = doublet of doublet, m = complex multiplet or wide signal.

of a white wax. The peaks assigned to R Binol-C_{22}**,** are listed as follows: ^{1}H NMR (500 MHz, $CDCl_3$, 20 °C): δ 0.88 (t, J = 6.4 Hz, 6H), 0.9 (m,4H), 0.99 (m, 8H), 1.09, (m, 4H), 1.26 (s, 60H), 1.38 (m, 4H), 3.91 (m, 4H), 7.14 (d, J = 9.3 Hz, 2H), 7.19 (t, J = 7.7 Hz, 2H), 7.29 (t, J = 6.3 Hz, 2H), 7.40 (d, J = 8.3 Hz, 2H), 7.84 (d, J = 8.4 Hz, 2H), 7.91 (d, J = 7.0 Hz, 2H) ppm. ^{13}C NMR (125 MHz, $CDCl_3$, 20 °C): δ 14.35, 22.93, 25.84, 29.39, 29.60, 29.63, 29.70, 29.74, 29.95, 32.16, 70.01, 116.11, 120.96, 123.58, 125.72, 126.21, 127.97, 129.21, 129.46, 134.44, 154.76 ppm.

3. Results and discussion

3.1. UV Visible spectroscopy of R Binol-C and R Binol-C_{22}

The normalized absorption spectra of R Binol, R Binol-C and R Binol-C_{22} are shown in figure 2. The spectrum of R Binol obtained in this study is similar to that of binaphthol diluted in Tetrahydrofuran (THF) in the work of Taupier [10]. The results showed that the form of absorption spectra of R Binol-C and R Binol-C_{22} molecules was similar to that of Binol. The absorption maxima, characteristic of R Binol, were then converted to new longer wavelengths. Red shift of the different absorption band was observed for the derivatives of R Binol [15]. The peak at 268 nm for Binol was shifted to 272 nm for the molecules of Binol-C and Binol-C_{22}, the peak at 278 nm for R Binol was shifted to 284 nm for molecules synthesized from R Binol, the peak at 289 nm of R Binol was shifted to 294 nm. The 320 nm peak of R Binol was shifted to 326 nm for R Binol-C and 328 nm for R Binol-C_{22}, the 333 nm peak of R Binol is shifted to 339 nm for Binol-C and 340 nm for R Binol-C_{22}.

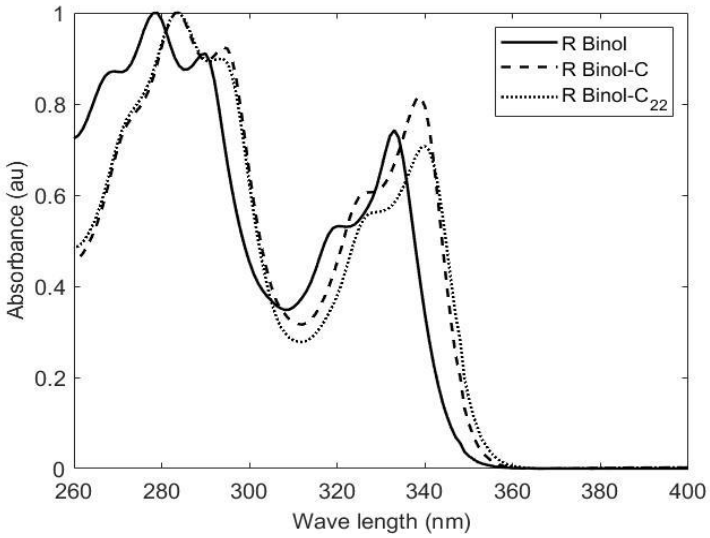

Fig. 2. UV Visible spectra of R Binol and derivatives (R Binol-C and R Binol-C_{22}) in solution in chloroform.

These shifts would be due to the displacements of the levels of electronic energies of the Binol molecule under the effect of the alkyl groups substituted on the oxygen atoms thus creating possible complexes of molecules. UV-Visible absorption maximum position is dependent upon the size and the shape of the complexes obtained from any conjugation [16]. The increasing of the particle size due to the increase in the conjugation of the system led to a red shift in the absorption spectra [17, 18, 19].

3.2. NMR spectroscopy of R Binol-C_{22}

NMR analysis was used to determine the structure of the derivative molecule. Figure 3 presents ^{1}H NMR spectra obtained for the R Binol-C_{22} sample at 500MHz. Other NMR spectra of R Binol-C and R Binol-C_{22} were provided as supplementary information to this paper (Appendix). The different NMR spectra obtained on the synthesized molecule made it possible to confirm their structure. Typical shift corresponding to alkyl chains can be found. Chemical shifts associated with the atoms of the two naphthalene groups can be observed [15].

In ^{1}H NMR spectrum (figure 3) the signal corresponding to hydroxyl groups disappeared, demonstrating that Binol hydroxyl groups were involved in bonding with carbonyl groups in the synthesis of R Binol-C_{22} molecule.

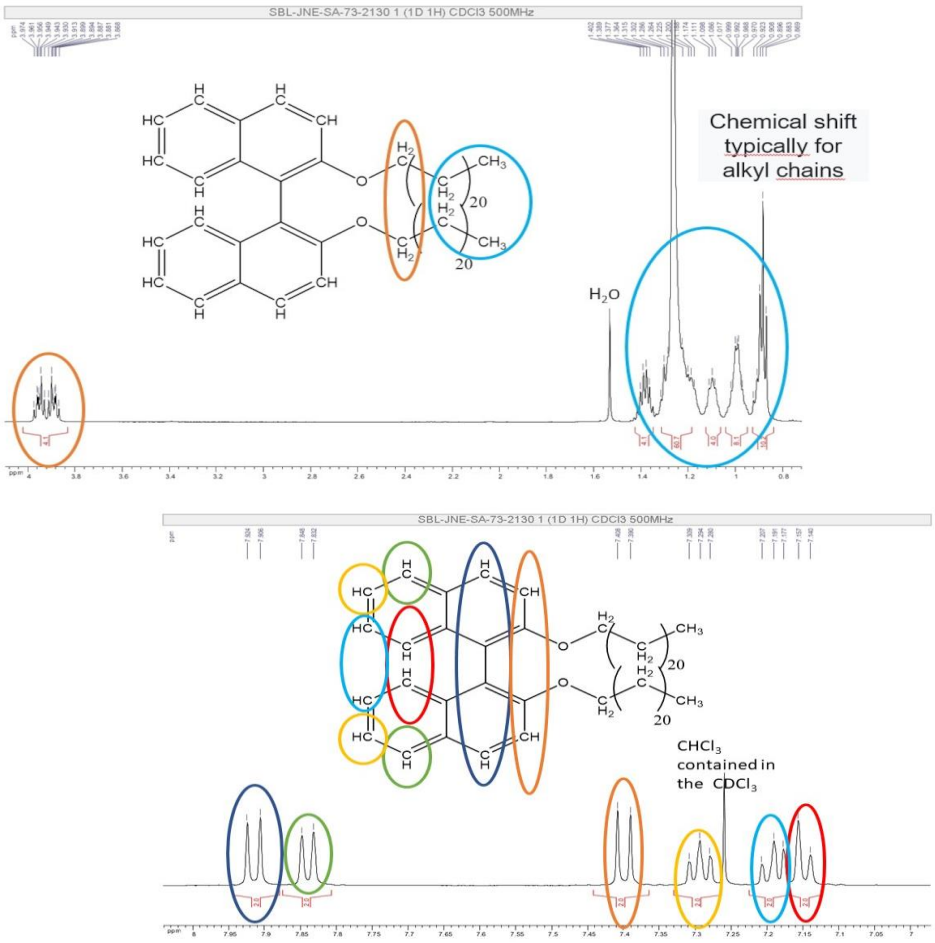

Fig. 3. ^{1}H NMR spectra obtained for the R Binol-C_{22} sample at 500MHz.

3.3. IR transmission and Raman spectroscopies of R Binol-C and R Binol-C_{22}

The changes in chemical bonds during the synthesis of the different derivatives molecules from R Binol were investigated using the IR and Raman spectra as shown in figures 4 and 5, respectively. New peaks appeared and certain peaks disappeared in the Raman and IR spectra. The analysis of the spectra of figure 4, according to the table associated with the various bands of the IR spectrum [20], shows a vibration of the group (-OH) bound (hydrogen bond) associated with the peak at 3429 cm^{-1} located between 3100 cm^{-1} and 3500 cm^{-1}. A vibration of the free (-OH) group is associated with the peak at 3507 cm^{-1} located between 3500 cm^{-1} and 3700 cm^{-1}. These two previous peaks were present on the R Binol spectrum and were absent on the R Binol-C and R Binol-C_{22} spectra, respectively. This confirms the disappearance of the -OH group in the two new molecules synthesized from Binol. Indeed, the hydrogen atoms of the (-OH) groups have been substituted by alkyl groups. New different peaks appeared in the spectra of the synthesized molecules as the bands at 2848 cm^{-1} and at 2915 cm^{-1} corresponding to the vibration modes of the C-H bond. These two bands are absent on the spectrum of Binol, weak on the spectrum of R Binol-C and very marked on the spectrum of R Binol-C_{22}.

The presence of a long carbon chain with several C-H bonds in R Binol-C_{22} explains the relative high intensity of these two bands in its spectrum compared to that of R Binol-C.

Raman spectra of R Binol and R Binol-C and R Binol-C_{22} were presented on figure 5. The spectrum obtained for R Binol corresponds well to that of the spectra in the references [21, 22]. Differences were observed between the spectra of Binol, R Binol-C and R Binol-C_{22}. The peak at 436 cm^{-1} present in the spectrum of R Binol has disappeared in the spectra of R Binol-C and of R Binol-C_{22}. The peak at 791 cm^{-1} present in the spectrum of Binol is no longer present in the spectra of R Binol-C and R Binol-C_{22}. The peak at 906 cm^{-1}, which appeared in the spectra of R Binol-C and R Binol-C_{22}, was not present on the spectrum of R Binol. The peaks at 1129 cm^{-1} and 1294 cm^{-1} are present only on the spectrum of R Binol-C_{22}, they are absent on the spectrum of R Binol as well as on the spectrum of R Binol-C. A broad band with a central peak at 2880 cm^{-1} is present on the spectrum of R Binol-C_{22} while this peak is absent on the spectra of R Binol and R Binol-C. The strongest band at 1379 cm^{-1} corresponding to C-O stretching were seen in the Raman spectra of R Binol while in its derivatives the band shifted to a smaller wavenumber. This position of C-O stretching band was found at 1381cm^{-1} in the reference [22]. Indeed, this peak is positioned at 1371 cm^{-1} for R Binol-C as well as for R Binol-C_{22}. These results are similar to that observed in reference [22]. The IR and Raman spectra have confirmed the synthesis of new molecules as derivatives of Binol.

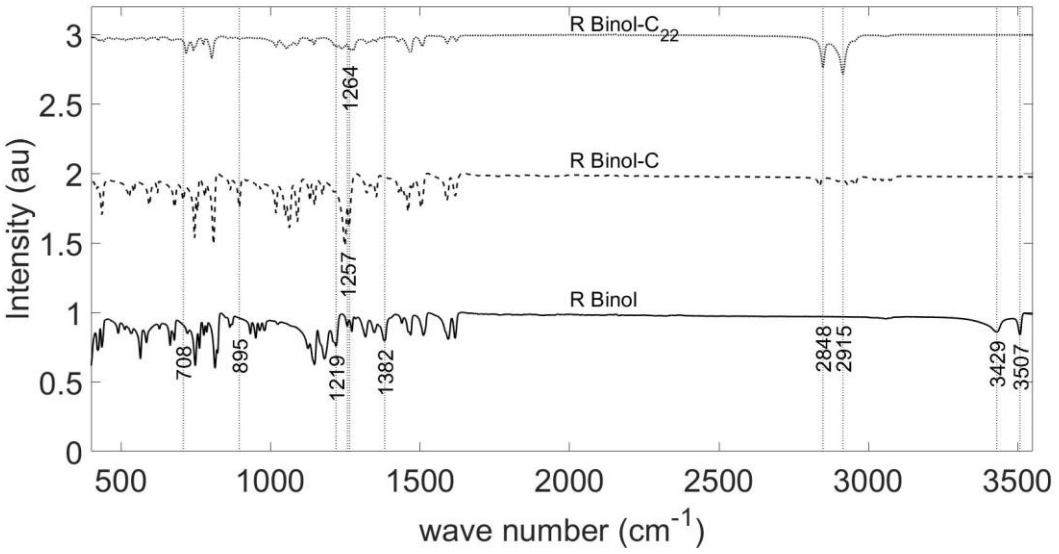

Fig. 4. IR spectra of R Binol and its derivatives.

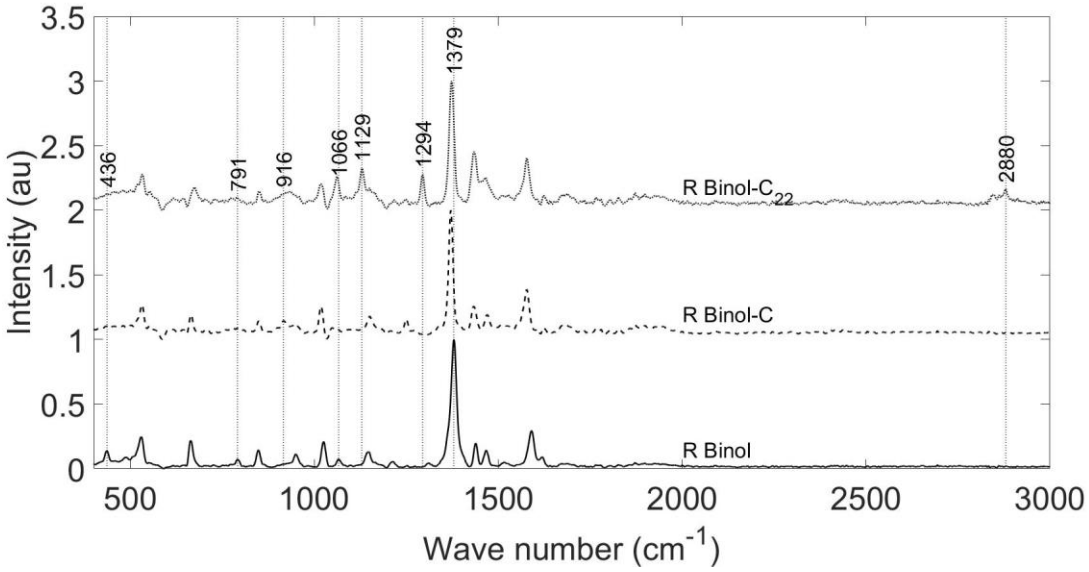

Fig. 5. Raman spectra of R Binol and its derivatives.

3.4. Sum-frequency generation signals in R Binol-C_{22}

The samples of the molecule obtained from substitution of hydrogen atoms by docosyl groups (R Binol-C_{22}) were investigated with the sum-frequency generation device set up. The derivative molecules obtained by substitution of hydrogen atoms by methyl groups (R Binol-C) could not be soluble and it was not used for SFG analysis. The chiral SFG spectrum and images of the sample were performed in the different configurations of the device.

3.4.1. Sum-Frequency spectrum

The figure 6.a presents the SFG spectrum generated by the molecule R Binol-C_{22} in

solution in Tetrahydrofuran (THF). The polar diagram (Figure 6.b) shows the polarization of the chiral SFG signal. The SFG signal at 300 nm corresponds to the sum of the frequencies of the two incident beams of respective wavelengths 900 nm and 450 nm. This sum-frequency signal is polarized perpendicular to the polarizations of the excitation beams and corresponds to the chiral SFG signal [23]. From the expression of the chiral SFG field generated as a function of the incident fields, the chiral SFG field is proportional to the vector product of the two incident fields, therefore, the SFG chiral signal is obtained in SPP configuration. Moreover, the surface SFG signal and the third harmonic generation signal which are also emitted at 300 nm and which were expected in the measurements of the chiral SFG are not expressed in the SPP configuration. That means only the electric dipole interaction led to chiral SFG signals [24]. The results obtained for this derivative molecule from Binol had shown that the chirality was preserved and that chirality always made it possible to generate the sum-frequency. Similar results were found by Lee et al. [25] and Belkin et al. [26] demonstrating vibrationally resonant optically active sum-frequency generation in chiral limonene liquids and in Binol [27] as a sensitive chirality probe.

The intensity of the measured chiral SFG signal was studied as a function of the powers of the two incident beams. Figure 7.a showed the different spectra of the beam powers at 900 nm ranging from 10 mW to 65 mW, the 450 nm beam power was fixed at 0.5 mW.

Figure 7.b shows the variation of the intensity of the obtained SFG signal as a function of the beam power at 900 nm. We noted that the intensity of the SFG signal was linearly dependent on the power of the beam at 900 nm. It had been demonstrated that the amplitudes and the phases of the signals were in function of excitation wavelength [28].

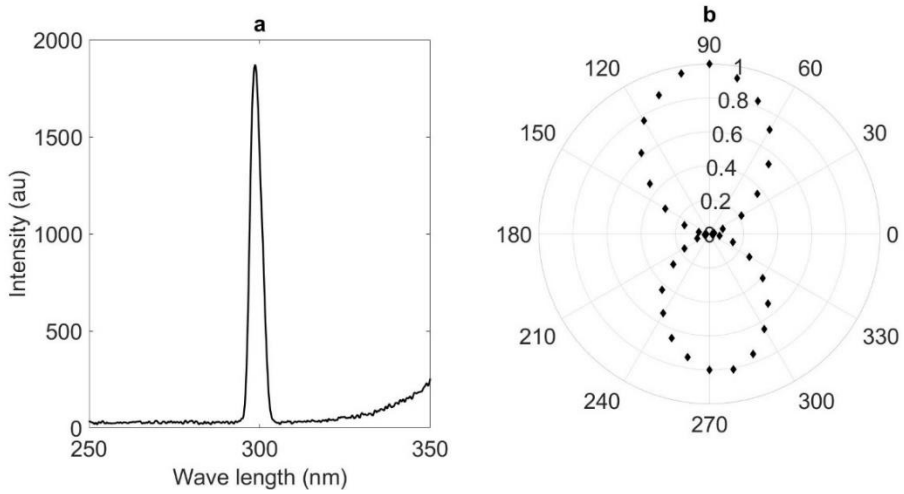

Fig. 6. (a) Chiral SFG spectrum of R Binol-C_{22} in liquid solution in THF; (b) Polar diagram associated with the spectrum.

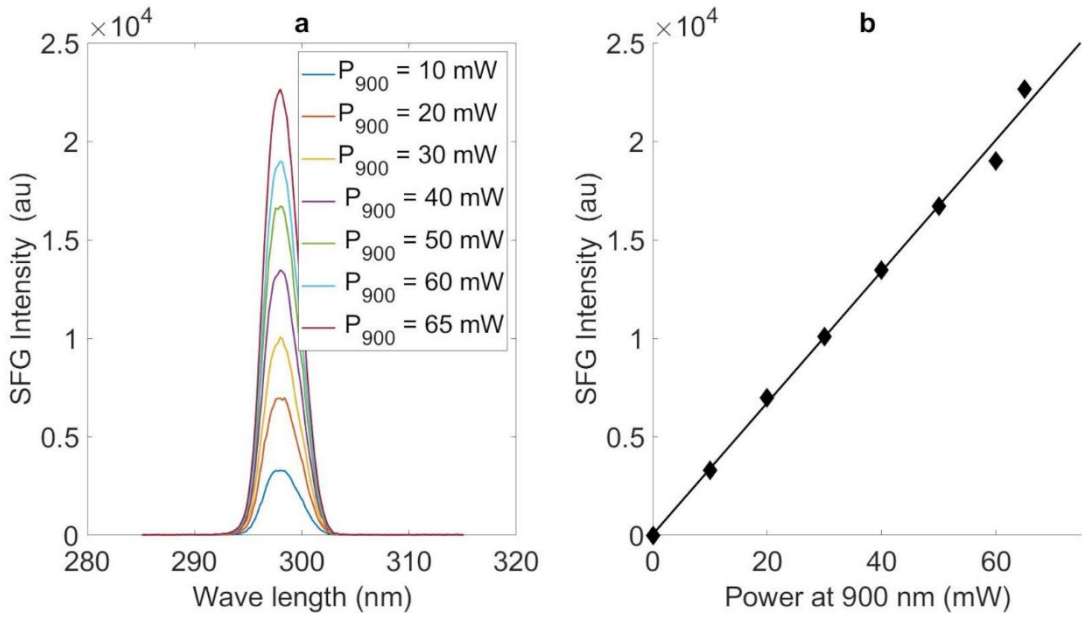

Fig. 7. (a) Chiral SFG spectra of R Binol-C_{22} as a function of beam powers at 900 nm; (b) SFG signal intensity as a function of beam power at 900 nm.

3.4.2. SFG imaging of R Binol-C_{22} sample

Images of a sample of liquid R Binol-C_{22} in solution in tetrahydrofuran were performed by the sum-frequency microscope set up. The liquid sample was inserted between slide and coverslips. Images of a portion of the sample of size of 100 µm by steps of 0.5 µm were presented on figure 8. The images were obtained point by point by a photomultiplier, the sample holder stage was moving with a step of 0.5 µm. Image (a) was taken in the SPP_zero configuration, image (b) in the SPP_out_zero configuration, image (c) in the PPP_zero configuration and image (d) in the PPP_out_zero configuration. In SPP_zero configuration, the signal obtained is the chiral SFG signal, in SPP_out_zero configuration, no signal was expected, in PPP_zero configuration, there would be superposition of the surface SFG signal and the third harmonic signal. In PPP_off_zero configuration, there would only be third harmonic signal. From figure 8, we noticed a contrast on the image (a). The light part represented the liquid sample of R Binol-C_{22} in THF and the dark part represented the vacuum. Only image (a) gave good contrast and demonstrating that SFG microscopy was sensitive to molecular orientation [29]. This means that the chiral SFG signal obtained in the SPP configuration made it possible to image chiral liquid media containing the molecules of R Binol-C_{22}. It is an advantage for this technique to take into account only chiral species and it would be a useful sensitive and selective tool to probe biological molecules [30].

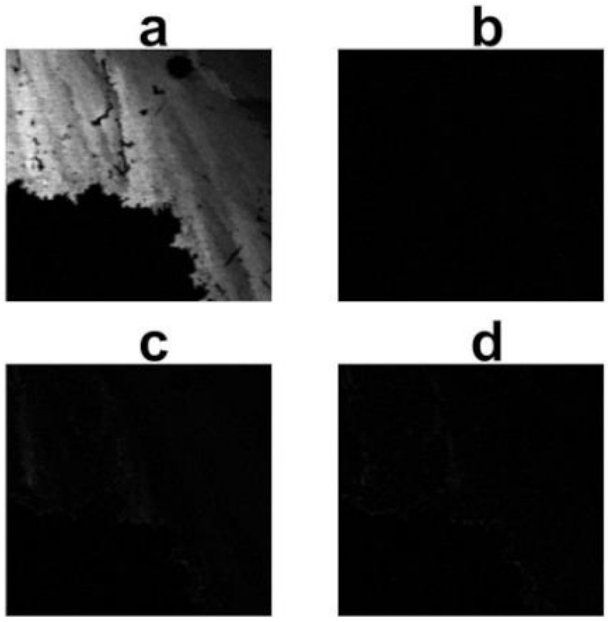

Fig. 8. Comparative contrast image of a sample of R Binol-C_{22} in solution in THF: (a) in SPP_zero configuration; (b) in SPP_off_zero configuration; (c) in PPP_zero configuration; (d) in PPP_off_zero configuration.

A similar result was obtained with the samples of R Binol which is not presented in the paper. The surface SFG signal generated in configuration PPP_zero and the THG signal in PPP_out_zero configuration were negligible and did not provide good imaging contrast on the sample. This comparison was made because all these signals were emitted in the same area of the sample. Indeed, the surface signal SFG and the signal THG were essentially emitted at the interfaces between two media. The chiral SFG signal was also emitted at the surface of the sample. When the entire interaction region was in chiral solution, the chiral SFG signal disappeared. The signal was then maximum when half of the effective interaction zone of the beams was in the sample.

This behaviour was due to the fact that the power of the SFG signal was of the form of Eq. (2) [31] :

$$P_{SFG} \alpha |J|^2 \quad \text{with} \quad J = \int_{-\infty}^{+\infty} \frac{\chi^{(2)} e^{i\Delta kbz}}{1+2iz} dz \qquad (2)$$

Where z represented the axial position with z = 0 corresponding to the focal plane, $\Delta\vec{k} = \overrightarrow{k_1} + \overrightarrow{k_2} - \overrightarrow{k_3}$ was the phase mismatch of the wave vectors and b is the focal zone depth. $\overrightarrow{k_1}$ et $\overrightarrow{k_2}$ were the wave vectors of the incident waves and $\overrightarrow{k_3}$ the wave vector of the SFG wave. The denominator in the integral J was a characteristic of the Gaussian beams propagation through the focal region. For an isotropic medium, it could be shown that J vanished when Δk was less than 0, which corresponds to the R Binol-C_{22} samples used in this study. Thus, when the focal region was entirely in solution, the SFG signal disappeared. When only half of the focal region was in solution, J was maximal, and therefore the SFG signal is maximal [31]. In order to know the region from where the SFG signals are generated the thickness of the interaction zone was assessed and XZ images (figure 9) were recorded in all the microscope configurations [32].

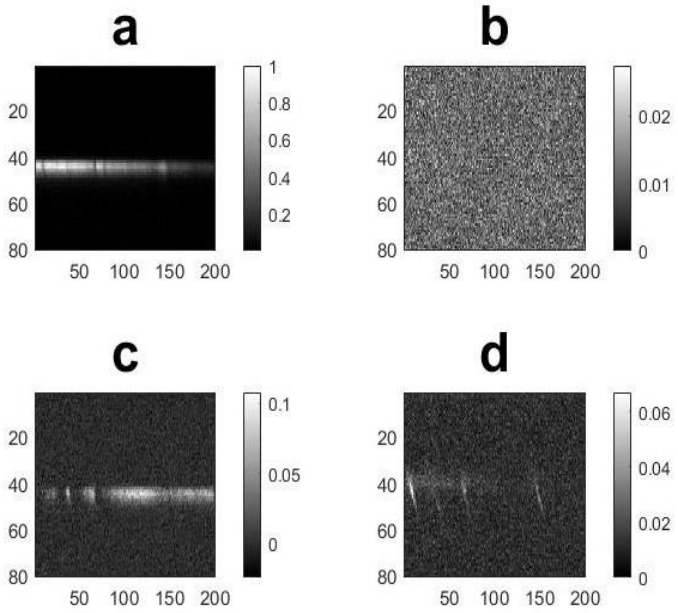

Fig. 9. Comparative XZ contrast image of a sample of liquid R Binol-C_{22} in solution in THF: (a) in SPP_zero configuration; (b) in SPP_non_zero configuration; (c) in PPP_zero configuration; (d) in PPP_non_zero configuration.

The four images were taken in the SPP_zero, SPP_hors_zero, PPP_zero and PPP_hors_zero configurations and were displayed to have the relative intensities of all the signals. On figure 9, a slight surface SFG and THG generation signal in PPP_zero configuration and a THG signal in PPP_hors_zero configuration could be observed. These different signals were emitted in the same area as the chiral SFG signal. The thickness of the chiral SFG generation zone was assessed and the intensity profile of the XZ image was plotted (Figure 10) to find the SFG sampling depth.

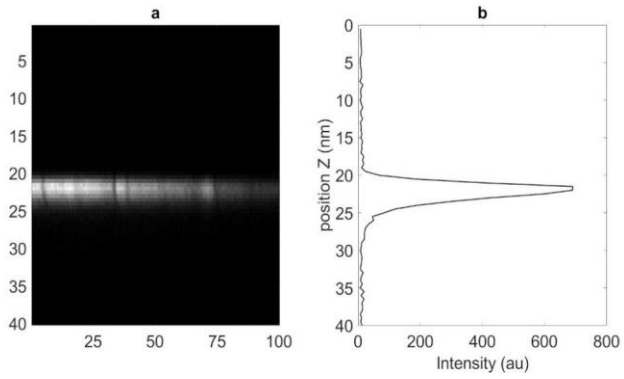

Fig. 10. (a) XZ image of a sample of R Binol-C_{22} in solution in THF in SPP zero configuration; (b) Corresponding intensity profile.

The profile showed an asymmetry of the interaction zone. The area at the top of the profile corresponded to the start of the SFG generation area. This zone corresponded to the contact of the sample with the coverslip. The lower part corresponded to the decrease in intensity in the sample due to the phase mismatch. The maximum intensity was obtained when half of the interaction voxel is in the sample.

4. Conclusion

Binaphthol and its derivatives fingerprints were performed using absorbance, IR-transmission and Raman spectroscopies. Sum-frequency measurements were carried out on the R Binol-C_{22} molecule in solution of THF. Chiral sum-frequency signals were obtained and the conservation of the chirality of the molecules was observed. The Raman and IR-transmission spectra clearly showed that (OH) chemical bonds disappeared and new bonds were created during the synthesis of the R Binol derivatives.

The results showed the efficiency of the determination of chirality using the sum-frequency generation technique. The information obtained on the chirality of these derivatives with the sum-frequency generation microscope demonstrated that this tool is a powerful imaging technique for chemistry in the synthesis and characterization of chiral molecules for therapeutic applications and biological samples.

Acknowledgements

The authors would like to thank the Service de Coopération et d'Action Culturelle (SCAC), the Swedish International Development Cooperation Agency (Sida) through the International Science Programme (ISP), Uppsala University and the African Spectral Imaging Network (AFSIN) for the financial support.

References

[1] I. Agranat, H. Caner, *Intellectual property and chirality of drugs*, Drug Discovery Today 4 (7) (1999) 313-321.

[2] I. Agranat, H. Caner, J. Caldwell, *Putting chirality to work: the strategy of chiral switches*, Nat. Rev. Drug Discovery 1(10) (2002) 753-768.

[3] A. Higuchi, M. Tamai, Y.-A. Ko, Y.-I. Tagawa, Y.-H. Wu, B. D. Freeman, J.-T. Bing, Y. Chang, Q.-D. Ling, *Polymeric Membranes for Chiral Separation of Pharmaceuticals and Chemicals*, Polymer Reviews 50(2) (2010) 113-143.

[4] R.W. Boyd, Nonlinear Optics, Third Edition. Academic Press, 3 edition ed., London (2008) 640.

[5] P.A. Franken, A.E. Hill, C.W. Peters, G. Weinreich, *Generation of Optical Harmonics*, Phys. Rev. Lett. 7(4) (1961) 118-119.

[6] P.-K. Yang, J. Y. Huang, *Sum-frequency generation from an isotropic chiral medium*, J. Opt. Soc. Am. B 15(6) (1998) 1698-1706.

[7] P.M. Rentzepis, J.A. Giordmaine, K.W. Wecht, *Coherent Optical Mixing in Optically Active Liquids*, Phys. Rev. Lett. 16 (1966) 792–794.

[8] X.D. Zhu, H. Suhr, Y.R. Shen, *Surface vibrational spectroscopy by infrared-visible sum frequency generation*, Phys. Rev. B 35(6) (1987) 3047-3050.

[9] Y.R. Shen, The Principles of Nonlinear Optics, ed., Wiley - Interscience, Hoboken, New Jersey (2002) 576.

[10] G. Taupier, Microscopie par génération de somme de fréquences optiques : application aux polymères de coordination chiraux, PhD Thesis, Université de Strasbourg, France (2016) 173.

[11] M.A. Belkin, S.H. Han, X. Wei, Y.R. Shen, *Sum-Frequency Generation in Chiral Liquids near Electronic Resonance*, Phys. Rev. Lett. 87(11) (2001) 113001.

[12] N. Ji, Y.-R. Shen, *A novel spectroscopic probe for molecular chirality*, Chirality 18(3) (2006) 146-158.

[13] L. Su, Synthesis of Chiral Binaphthol Derivatives and their Applications in Asymmetric Alkylation Sulfoxidation and Conjugate Addition, PhD Thesis, Hong Kong Polytechnic University, China (2003) 202.

[14] A. Reddy Ankireddy, K. Paidikondala, R. Syed, R. Gundla, Ch. Venkata Ramana Reddy, T. Ganapathi, *Synthesis of Chiral 3,3'-Disubstituted (S)-BINOL Derivatives via the Kumada and Suzuki Coupling and Their Antibacterial Activity*, Russ. J. Gen. Chem. 90 (2020) 1507–1517. https://doi.org/10.1134/S1070363220080198.

[15] M. Flegel, M. Lukeman, P. Wan, *Photochemistry of 1,1'-bi-2-naphthol (BINOL) — ESIPT is responsible for photoracemization and photocyclization*, Canadian Journal of Chemistry 86(2) (2008) 161–169. https://doi.org/10.1139/v07-143.

[16] Interpreting Ultraviolet Spectra- The Effect of Conjugation (2021). Available from: https://chem.libretexts.org/@go/page/31556.

[17] N.S. Pesika, K.J. Stebe, P.C. Searson, *Relationship between Absorbance Spectra and Particle Size Distributions for Quantum-Sized Nanocrystals*, The Journal of Physical Chemistry B 107(38) (2003) 10412-10415.
DOI: 10.1021/jp0303218.

[18] H. Kato, A. Nakamura, K. Takahashi, S. Kinugasa, *Size effect on UV-Vis absorption properties of colloidal C60 particles in water*, Physical Chemistry Chemical Physics 11(25) (2009) 4946-4948. doi:10.1039/b904593g.

[19] A.S. Ogunlaja, E. Hosten, R. Betz, Z.R. Tshentu, *Selective removal of isoquinoline and quinoline from simulated fuel using 1,1'-binaphthyl-2,2'-diol (BINOL): crystal structure and evaluation of the adduct electronic properties*, RSC Adv. 6 (2016) 39024-39038. https://doi.org/10.1039/C6RA03854A.

[20] J. Coates, Interpretation of Infrared Spectra, A Practical Approach. In Encyclopedia of Analytical Chemistry (eds R.A. Meyers and M.L. McKelvy) (2006).
https://doi.org/10.1002/9780470027318.a5606.

[21] Z. Li, D. Chen, T. He, F. Liu, *UV Near-Resonance Raman Spectroscopic Study of 1,1‘-Bi-2-naphthol Solutions*, J. Phys. Chem. A 111(22) (2007) 4767-4775.

[22] H. I. Nogueira, S. M. Quintal, *Surface-enhanced Raman scattering (SERS) studies on 1,1'-bi-2-naphthol*, Spectrochimica acta. Part A, Molecular and biomolecular spectroscopy 56(5) (2000) 959-64.
doi:10.1016/s1386-1425(99)00189-4.

[23] P. Fischer, F.W. Wise, A.C. Albrecht, *Chiral and achiral contributions to sum-frequency generation from optically active solutions of binaphthol,* J. Phys. Chem. A 107 (2003), 8232-8238.

[24] P. Fischer, K. Beckwitt, F.W. Wise, A.C. Albrecht, *The Chiral Specificity of Sum-Frequency Generation in Solutions*, Chem. Phys. Lett. 352 (2002) 463–468.

[25] T. Lee, H. Rhee, M. Cho, *Femtosecond Vibrational Sum-Frequency Generation Spectroscopy of Chiral Molecules in Isotropic Liquid*, The Journal of Physical Chemistry Letters 9(23) (2018) 6723-6730.
DOI: 10.1021/acs.jpclett.8b02947.

[26] M.A. Belkin, T.A. Kulakov, K.-H. Ernst, L. Yan, Y.R. Shen, *Sum-Frequency Vibrational Spectroscopy on Chiral Liquids: A Novel Technique to Probe Molecular Chirality*, Phys. Rev. Lett. 85 (2000) 4474.
https://doi.org/10.1103/PhysRevLett.85.4474

[27] M.A. Belkin, Y.R. Shen, *Doubly Resonant IR-UV Sum-Frequency Vibrational Spectroscopy on Molecular Chirality*, Phys. Rev. Lett. 91 (2003) 213907.
https://doi.org/10.1103/PhysRevLett.91.213907.

[28] M. Okuno, D. Ishikawa, W. Nakanishi, K. Ariga, T. Ishibashi, *Symmetric Raman Tensor Contributes to Chiral Vibrational Sum-Frequency Generation from Binaphthyl Amphiphile Monolayers on Water: Study of Electronic Resonance Amplitude and Phase Profiles*, The Journal of Physical Chemistry C 121(21) (2017) 11241-11250.
DOI: 10.1021/acs.jpcc.6b12664.

[29] A. Hanninen, M. Wai Shu, and E. O. Potma, *Hyperspectral imaging with laser-scanning sum-frequency generation microscopy*, Biomedical optics express 8(9) (2017) 4230–4242. https://doi.org/10.1364/BOE.8.004230.

[30] N. Ji, K. Zhang, H. Yang, Y.-R. Shen, *Three-Dimensional Chiral Imaging by Sum-Frequency Generation*, Journal of the American Chemical Society 128(11) (2006) 3482-3483. DOI: 10.1021/ja057775y.

[31] N. Ji, Sum-Frequency Generation from Chiral Media and Interfaces, PhD Thesis, University of California, Berkeley, USA (2005) 155.

[32] C.M. Lee, K. Kafle, S. Huang, S.H. Kim, *Multimodal Broadband Vibrational Sum Frequency Generation (MM-BB-V-SFG) Spectrometer and Microscope*, The Journal of Physical Chemistry B 120(1) (2016) 102-116. DOI: 10.1021/acs.jpcb.5b10290.

Appendix

- **General methods:**

^{1}H and ^{13}C {^{1}H}, nuclear magnetic resonance (NMR) spectra were recorded on a Bruker Avance III HD - 500 MHz. ^{13}C assignments were confirmed when necessary with the use of DEPT 135 experiments. ^{1}H and ^{13}C-NMR spectra were referenced using the residual solvent peak ($CDCl_3$: δ H = 7.26 ppm; δ C = 77.16 ppm) at 295K. Chemical shifts δ are given in ppm whereas coupling constants J are stated in Hertz (Hz). The following abbreviations are used to classify the multiplicity of the observed signals: s = singlet, d = doublet, t = triplet, dd = doublet from doublet, m = complex multiplet or broad signal.

- **^{1}H and ^{13}C NMR spectra**

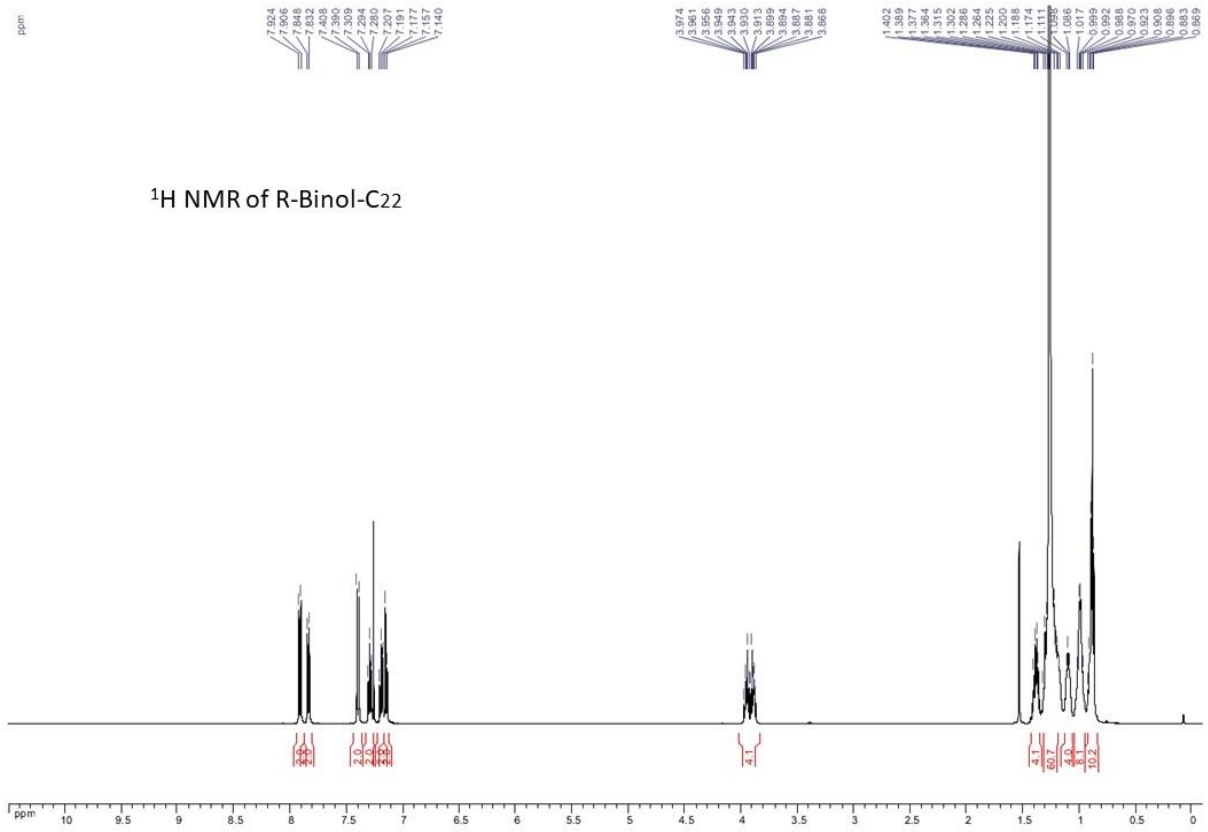

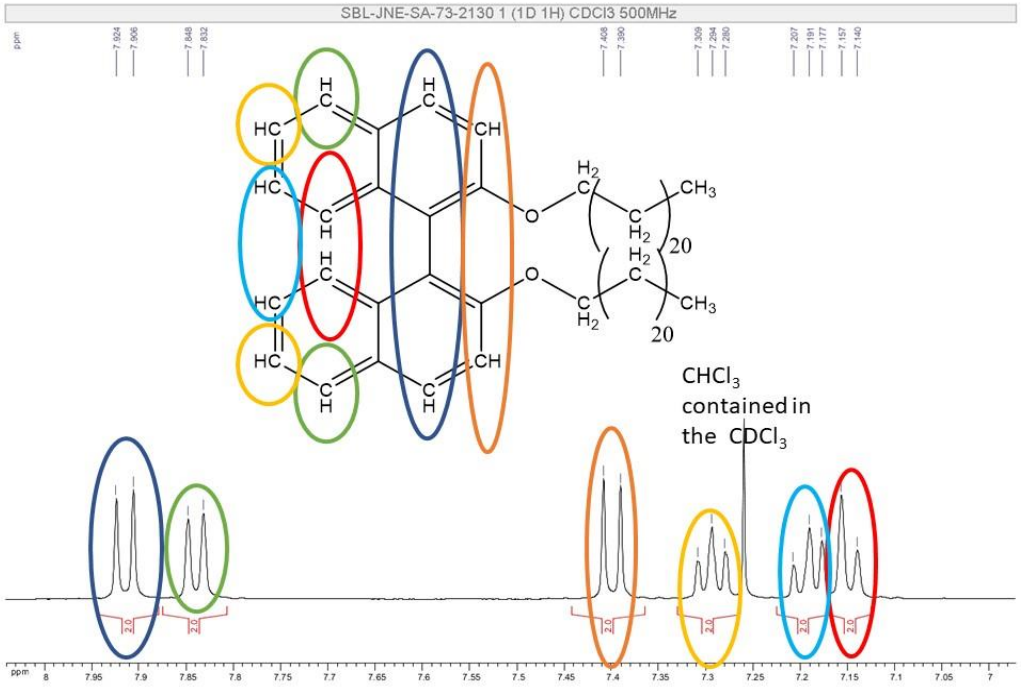
SBL-JNE-SA-73-2130 1 (1D 1H) CDCl3 500MHz
CHCl3 contained in the CDCl3

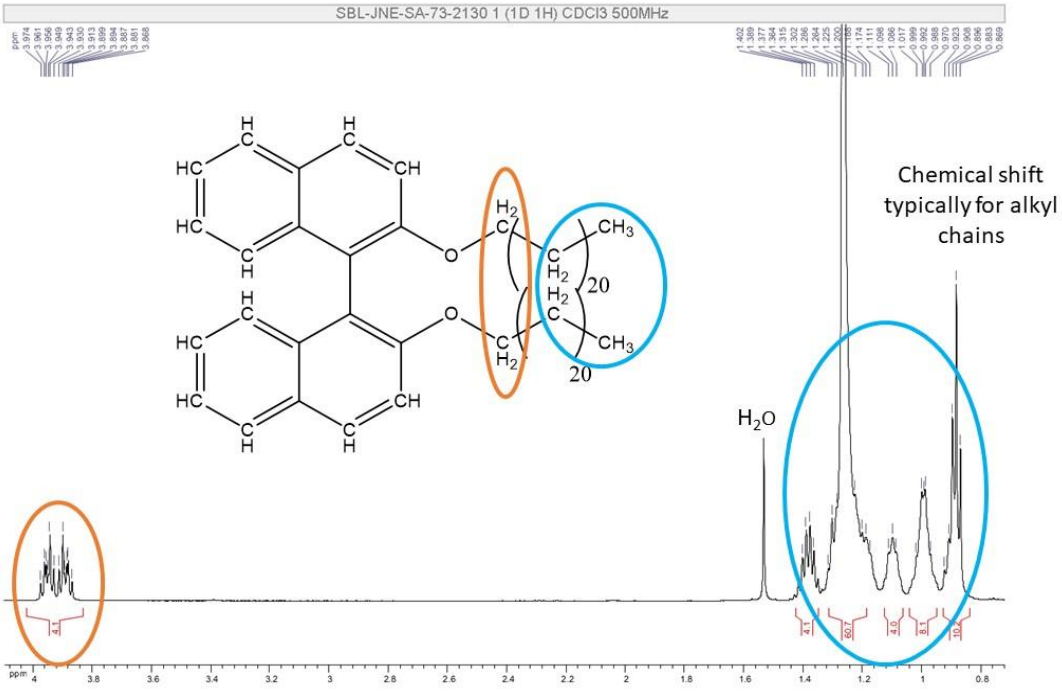
SBL-JNE-SA-73-2130 1 (1D 1H) CDCl3 500MHz
Chemical shift typically for alkyl chains
H2O

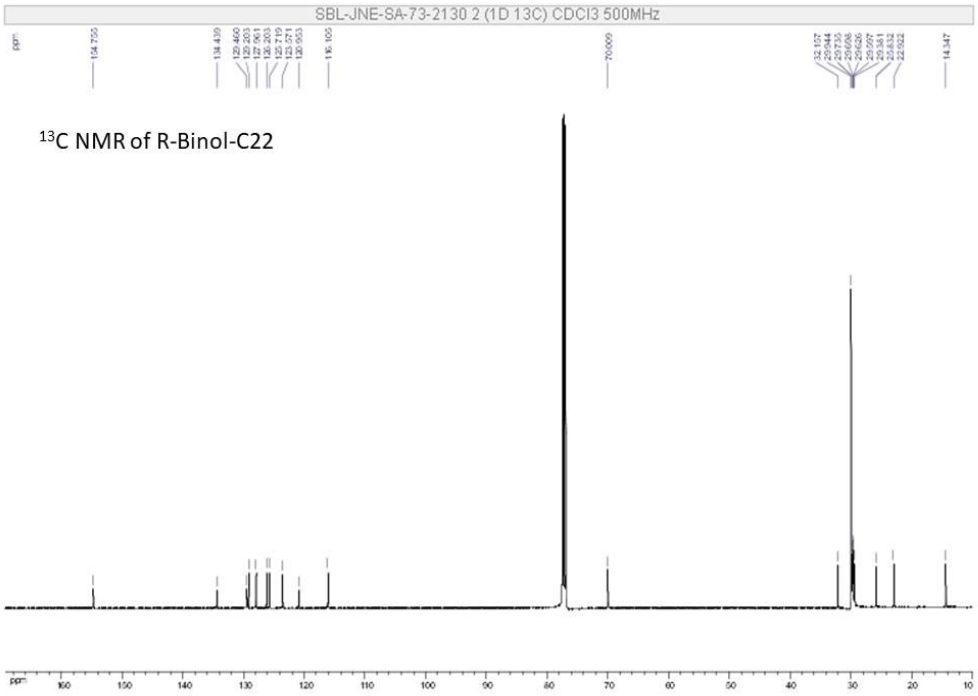
SBL-JNE-SA-73-2130 2 (1D 13C) CDCl3 500MHz
^{13}C NMR of R-Binol-C22

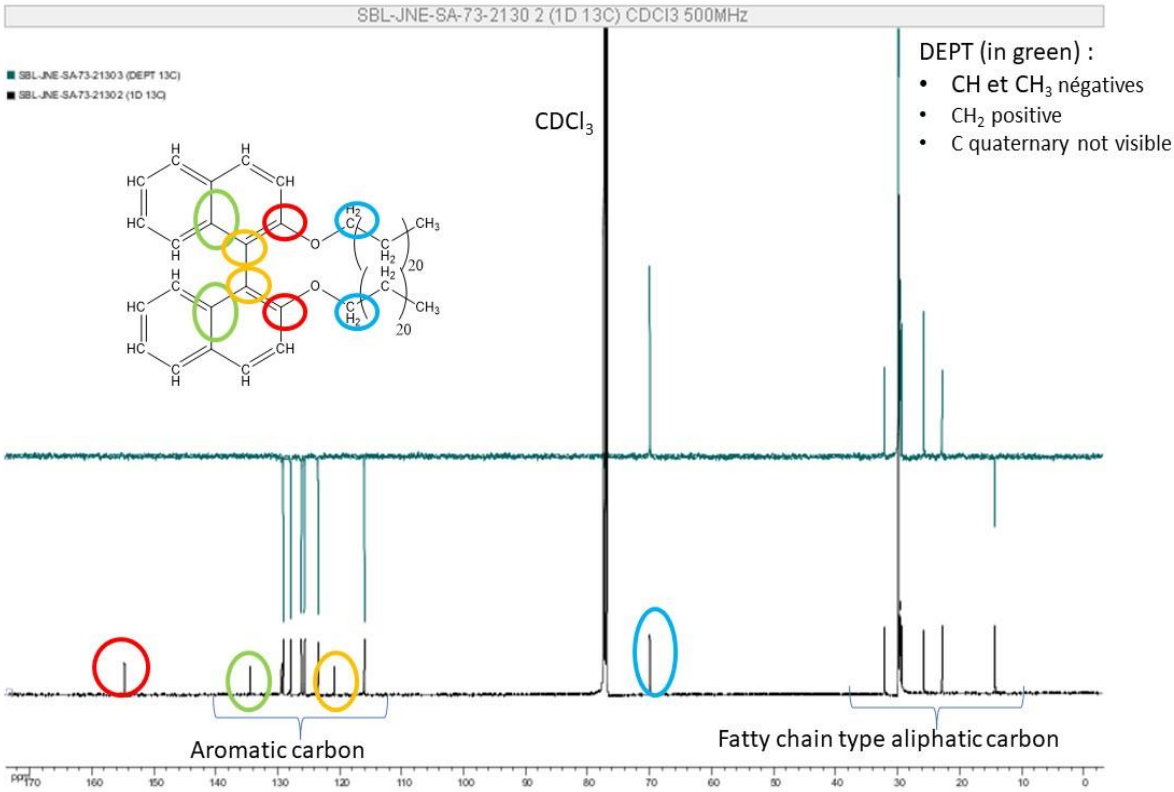
SBL-JNE-SA-73-2130 2 (1D 13C) CDCl3 500MHz
SBL-JNE-SA-73-21303 (DEPT 13C)
SBL-JNE-SA-73-21302 (1D 13C)
CDCl3
DEPT (in green) :
• CH et CH3 négatives
• CH2 positive
• C quaternary not visible
Aromatic carbon
Fatty chain type aliphatic carbon

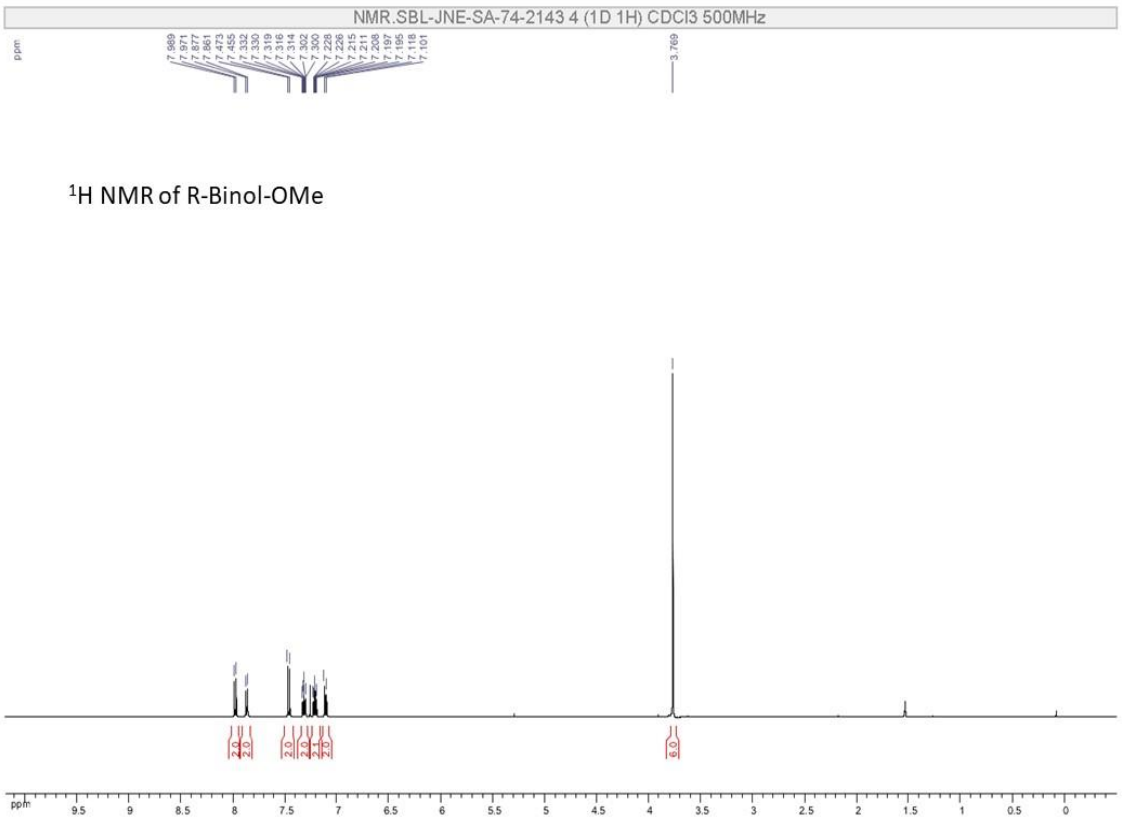

^{1}H NMR of R-Binol-OMe

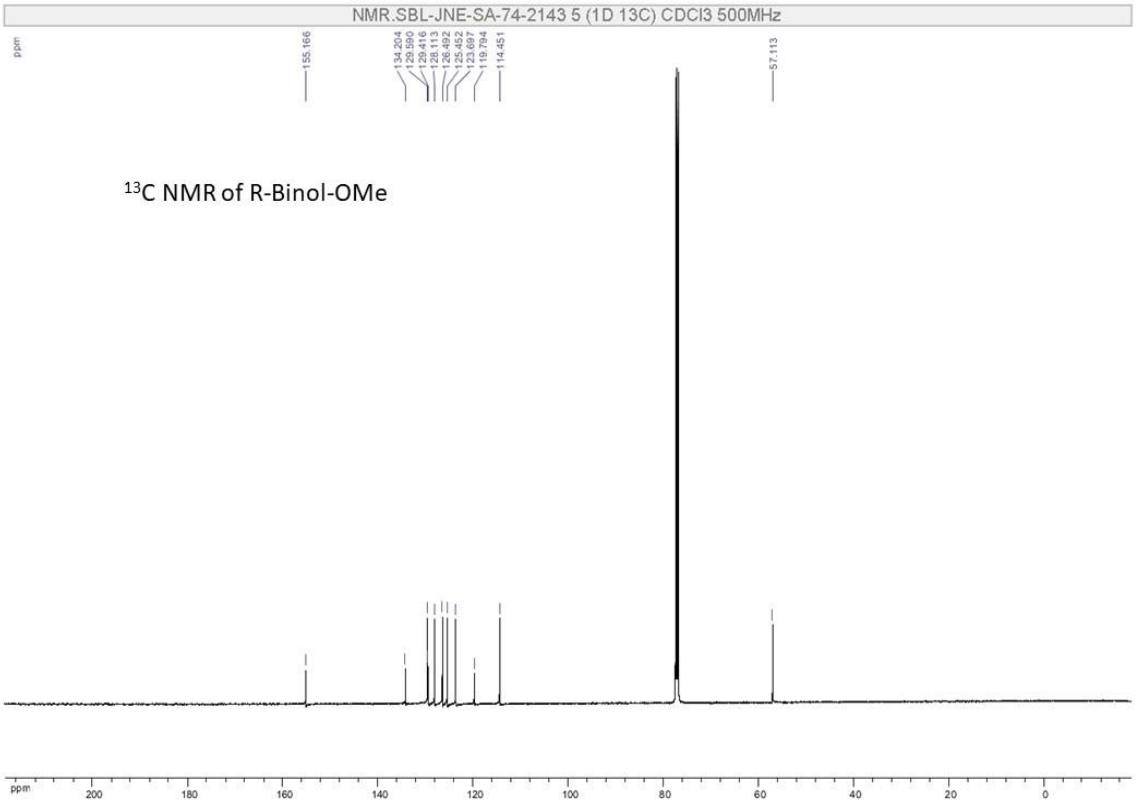

^{13}C NMR of R-Binol-OMe